1-1-2003

Femtosecond pulsed laser deposition and patterning of thin films for MEMS

Michael Joseph Stock
Iowa State University

Femtosecond pulsed laser deposition and patterning of thin films for MEMS

by

Michael Joseph Stock

A thesis submitted to the graduate faculty
in partial fulfillment of the requirements for the degree of
MASTER OF SCIENCE

Major: Mechanical Engineering

Program of Study Committee:
Pal A. Molian, Major Professor
Gary L. Tuttle
Daniel B. Bullen

Iowa State University
Ames Iowa,
2003

Graduate College

Iowa State University

This is to certify that the master's thesis for

Michael Joseph Stock

has met the thesis requirements of Iowa State University

Signatures have been redacted for privacy

TABLE OF CONTENTS

ABSTRACT

An investigation was undertaken to determine the effects of energy fluence, polarization, pulse width, machining speed, and material properties on pulsed laser deposition (PLD) and laser micromachining of ultra hard Al MgB_{14}.

In this work, a 120-fs pulsed, 800-nm wavelength Ti: Sapphire laser was used for deposition and micromachining thin films of ultra-hard $AlMgB_{14}$, and polysilicon thin films on a silicon substrate. Polysilicon was first deposited by low-pressure chemical vapor deposition followed by Al MgB_{14} using femtosecond pulsed laser deposition. The features were examined and corelated to the experimental variables to determine the most effective means of producing quality features. Two dimensional and stereo SEM micrographs were used to evaluate the resulting quality of the features.

In addition to the machined features, the quality of the deposited film was also evaluated to determine the best method of producing the desired features. The thin film is evaluated by X-ray photoelectron spectroscopy, X-ray diffraction, atomic force microscope, and nanoindentation. The results were also compared with nanosecond pulsed KrF excimer laser-deposited films.

CHAPTER 1. GENERAL INTRODUCTION

Introduction

Many techniques have recently emerged to produce MEMS devices. Each of these methods provides different advantages/disadvantages such as batch processing, material selectivity, and feature quality. While laser micromachining is a serial process that may prove to be an inefficient method of manufacture, it does allow materials to be machined in combinations that are not possible by other means. In this case a chemically stable ultra-hard material, Al MgB_{14}, is used as a structural member in a MEMS device. This paper will provide lessons learned in these experiments as a set of guidelines to successfully machine a thin film of this new material in combination with polysilicon.

Thesis Organization

This report reviews the issues of laser micromachining by presenting the findings in two papers by this author, and supplementing with a discussion of further findings including a consolidation of ideas in the final chapter. Each section lists a relative list of references, tables, and figures so as to preserve each paper as presented in its respective publication.

CHAPTER 2:FEMTOSECOND PULSED LASER PROCESSING OF THIN FILMS FOR MEMS DEVICES

Proceedings of International Congress on Applications of Lasers and Electro-Optics, ICALEO (LIA) 2002

Michael Stock, Pal Molian, Christian Zorman

Abstract

Microfabrication of MEMS devices involving deposition and surface micromachining of thin films is becoming an increasingly complex process due to the multi-layers and difficult-to-etch materials. Laser microfabrication is an excellent alternative to the traditional wet and dry chemical etching techniques especially for chemically resistant materials. In this work, a 120-fs pulsed, 800-nm wavelength Ti: sapphire laser was used for micromachining thin films of ultra-hard $AlMgB_{14}$ and polysilicon thin films on silicon substrate. Polysilicon was first deposited by low-pressure chemical vapor deposition followed by boride using femtosecond pulsed laser deposition. Channels were then machined in the thin films to pattern a device that would produce a linear resistance/deflection curve. Results show that the ultrafast laser has precisely ablated the thin films. However, the high-energy fluence used in single-pass surface micromachining enabled the formation of recast layer from the melting of silicon substrate. Multi-pass surface micromachining at low energy fluences eliminated the recast layers and produced clean features. Ultrafast laser micromachining is certainly beneficial over wet and dry etching in reproducibility, material choice, and minimal number of processing steps. However, the cleanliness remains to be improved.

Introduction and Background

MicroElectroMechanicalSystems (MEMS), the electronic chips with moving parts, grew out of the integrated circuit (IC) industry for a projected $34 billion market in 2002 [1]. Examples of MEMS devices include sensors, actuators, accelerometers, and miniature robots. These devices have captured the imagination of design engineers and are now being fabricated in industrial quantities for a variety of technological and medical end users.

Lasers are finding increasing uses in the microfabrication of MEMS structures. These include micromachining, modification of embedded surfaces, and rapid prototyping especially of oxide materials. Lasers are excellent tools for producing microstructures with increasing efficiency by ablation and deposition in conjunction with advanced lithography (LIGA) techniques.

Micromachining refers to the ability to create features in the range 1 μm and 1 mm [2]. Lasers have been proven to be effective tools for micromachining [3-6], although they battle with wet and dry chemical etching technologies. Lasers are suitable for applications that demand more precision, high speed, and "direct write" capability, and are environmentally friendly. Chemical etching processes are not fully satisfactory because they involve several steps, are useful for only silicon and metals, and are prone to environmental-disposal problems.

The growing demands of industry require that the method of producing microstructures must be capable of processing new and traditionally difficult-to-machine materials. Lasers can work on soft, hard, tough, and brittle materials and hence are useful to emerging MEMS materials like SiC, Si_3N_4, PMMA and others. As a result, the use of lasers in micromachining has become vital in many sectors of industry that use specialized materials, such as non-conductive, superhard, or multilayer materials with strong chemical properties.

Laser micromachining offers new growth opportunities for fabricating numerous devices including diaphragms, grooves, orifices, cavities, springs, gears, linkages, and micromotors, which are then used for fabricating microsensors and microactuators with integrated electronics. Excimer lasers are widely used for micromachining applications that include photoablation, chemical etching, lithography, and surface cleaning. However, thermal damage and the size capability limit, the use of excimer laser for next generation MEMS devices, which will be less than 1 μm, and for which the ultrafast lasers would be well suited. Two excellent review articles [7,8] provide substantial information on the applications and capabilities of ultrafast lasers. The reviews indicate that high spatial resolution cannot be achieved in ns-pulsed excimer lasers because of thermal effects and the plasma formation above the surface. By reducing the pulse width in the fs-range, it is possible to alleviate both of these deleterious effects. Examples show excellent quality holes with straight walls, clean cuts, smooth walls, and an absence of thermal cracking [7-10]. Potential applications of ultrafast lasers include precision drilling and cutting of sub-micron

features for the microelectronics/medical industry, pulsed laser deposition of thin films, and desorption of water molecules in MEMS to prevent "stiction" failure [7-10].

The unique characteristic of the femtosecond pulsed lasers is the multiphoton excitation of materials that enables the micromachining process to become non-thermal and establishes accurate energy thresholds. Hence, by controlling the light intensity right above threshold only at the center of spot, a feature size less than spot itself could be produced. Other benefits of ultrafast lasers over long pulse lasers for micromachining are a much reduced heat-affected zone (HAZ), high efficiency (no plume interference) and no wavelength dependence. The reason for the reduced HAZ is that the interaction time of the pulse is faster than the time required for heat diffusion mechanisms. Another promising application of femtosecond lasers is surface micromaching of thin films. Traditional surface micromachining depends on some chemical methods including wet etching, dry etching, and reactive ion etching (RIE). The etch rates of these methods are low, and the absence of proper etchants also limit these processes to one layer in multi-layer chips.

In this paper, the results of femtosecond laser microfabrication of ultra-hard boride ($AlMgB_{14}$) and polysilicon thin films on silicon substrate are presented. Laser deposition of boride followed by laser surface micromachining was performed to produce channels in the films that outline a device profile.

Experimental Materials and Procedures

In the traditional sense, surface micromachining involves structural and sacrificial layers. The structural layers are those in which the final microstructures are made while the

sacrificial layers are those that separate the structural layers and are eventually removed in the final device fabrication. Most of the efforts in surface micromachining were based on polysilicon /silicon dioxide material system because of its widespread use in IC fabrication technology. Recently silicon nitride and aluminum were used as sacrificial layers in conjunction with polysilicon. Silicon nitride has also been attempted as a structural material with polysilicon serving as the sacrificial material. The structural layers must exhibit the desired electrical and mechanical properties including electrical resistivity, band gap, high yield and fracture strengths, minimal creep and fatigue, low friction and wear properties.

In this work, we chose a material system of polysilicon and $AlMgB_{14}$, both serving as structural layers. Polysilicon has been attractive as a structural material because it has good mechanical properties, comparable to single crystal silicon. Polysilicon micromechanical devices such as cantilevers and micromotors have been well known. $AlMgB_{14}$ is a new material for MEMS and was first studied more than 30 years ago. It has been the subject of renewed interest due to its extreme hardness and high chemical stability [11, 12]. The hardness of $AlMgB_{14}$ containing 5 to 30 mol% additives lies in the range 35-46 GPa, which is comparable to the hardness of cubic-BN. Hot-press sintered $AlMgB_{14}$ exhibits an electrical conductivity of approximately 80 to 1500 $\Omega^{-1}m^{-1}$ compared to that of silicon, which is $.4(10^{-3})$ $\Omega^{-1}m^{-1}$, and high-purity crystal show evidence of hopping conduction [13]. The $AlMgB_{14}$ single crystals show p-type semiconducting behavior and can be overcompensated to n-type by doping with a variety of different metal atoms [14]. More recent tests suggested that $AlMgB_{14}$ might possess very high thermal conductivity [15]. Due to its novel

mechanical, electrical, and thermal properties, $AlMgB_{14}$ is a promising structural material candidate for applications in MEMS.

In this work, 2-μm thick layers of polysilicon were deposited on Si <100> wafers by low-pressure chemical vapor deposition (LPCVD). The details of this deposition process, a standard process in the microelectronics industry, may be referred to elsewhere [16]. About 1-μm thick of $AlMgB_{14}$ was then deposited on the polysilicon films by the femtosecond pulsed laser ablation in a vacuum chamber (10^{-6} torr) at 500°C substrate temperature. The substrate heating allowed better adhesion and alleviated the residual stresses in the resulting film. This process was carried out with pulse energy of 0.3 mJ for 1 hour, which produced an average film thickness of 1 μm. Among the several physical vapor deposition (PVD) techniques (e.g. thermal evaporation, sputtering, etc.), pulsed laser deposition (PLD) was found to be a good method to deposit $AlMgB_{14}$ films because of congruent ablation and emission of high kinetic energy species, both of which lead to stoichiometric films of complex, multicomponent boride [17].

An 800-nm wavelength, 1.0 mJ Ti:sapphire oscillator-amplifier system (Spectra-Physics, Model Hurricane X) based on a chirped-pulse-amplification (CPA) technique was used to ablate boride target for deposition. This CPA Ti:Sapphire system comprised of a pulse stretcher, a regenerative amplifier that is pumped by a Nd:YLF laser, and a compressor. The laser emitted 120 fs pulses of linearly polarized light with near Gaussian beam (M^2=1.5) at a central wavelength of 800-nm (photon energy = 1.55 eV). The nominal beam diameter was 6 mm. In the deposition experiment, the laser was operated in continuous-shot mode at

pulse frequencies of 1 kHz. The beam was focused on the target for a spot size of 150 μm using a 127-mm focal length lens.

The same femtosecond pulsed laser was again used for micromachining thin films. Here the beam, steered through a 45° reflective mirror and focused using a reflective objective lens with 0.4 NA and 14.5 mm working distance, was incident perpendicular to the sample surface. A quarter wave plate was employed for changing linearly polarized light into circularly polarized light to provide symmetric cutting capabilities in all directions. The spot size of the beam on the sample surface was about 3-μm. The pulse energy was set at 0.1 to 0.25 mJ. The samples were cleaned with methanol and mounted on a motorized x-y stage (Coherent LabMotion Series), which has a repeatability of 1 μm and a resolution of 1 μm. The number of laser pulses was controlled by an electronic shutter (UNIBLITZ VMM-T1), which incorporates two precise timers to control shutter exposure and delay intervals. Figure 1 shows the laser system (Spectra Physiscs Model Hurricane X) and focusing apparatus.

Following micromachining, a scanning electron microscope (SEM) (JEOL JSM 840, 10 kV accelerating voltage) operated in the secondary electron mode, and the associated energy dispersive X-ray spectrometer, were used to examine the laser machined features and analyze the compositions of debris and recast layer.

Principle of Device Operation

The goal of this design is to produce a device (Figure 2) that could linearly measure micron scale movement, strain, or gas flow. In addition since the device operates only based on the changes in resistance, the initial temperature-dependent resistance is irrelevant in the

deflection measurement. The idea stemmed from the design of a linear spring that produces a linear force/deflection curve. The force returned by the device is directly related to the strain, which means that if the change in resistance were measured, the resulting resistance change would also be linear with respect to deflection. The governing equation for resistive strain gages is as follows:

$$\mathbf{dR/R=S\varepsilon}$$

where R = resistance, ε = strain, and S=strain sensitivity index.

For the operation of this device, the contacts in the upper left-hand corner of Figure 2 are connected and the device is anchored along the length on the left-hand side. Once connected the resistance is measured over the effective length of the device, approximately 40 mm. Displacement is then measured by subtracting the initial resistance from the displacement resistance. For this reason, the direction of the displacement is also known by the polarity of the resistance change. This is a common flaw with standard resistance strain gauges because compressive strains cause delamination of the device. A similar device, known as Fan's cantilever, uses a vernier reading [16]. The cantilever measures strain by measuring the lateral contraction, changes in height, or rotation. The design is similar to the proposed design above but is circular and does not have a return loop because no electrical current is used.

Results and Discussion

Figure 3 shows the SEM micrograph of deposited boride film and particles with diameters ranging from less than 1 μm to a maximum of 4 μm. These particles were ejected

from the target surface during deposition. Attempts were made to reduce the diameter and frequency of these particles by decreasing the laser power and increasing the target-substrate distance. This in turn reduced the material removal rate from the target, and the deposition rate on the substrate surface. When the amount of material being removed is reduced, the expelled material is composed of smaller particles because only the material directly and intensely illuminated by the laser is expelled.

Figure 4 shows the energy dispersive X-ray spectrum of the film, showing the presence of Al, Mg and B. This type of measurement system allows X-rays to penetrate thin films, measuring substrate composition. This is the reason for the large silicon peak and an unmarked peak that corresponds to the presence of oxygen. Figure 5 shows the single-pass micromachined channels in the samples. The energy fluences required for acceptable micromachining of polysilicon and boride thin films are relatively lower (about five times) compared to the bulk silicon. Thus, boride and polysilicon films are quickly and easily laser machinable. However, one has to use very low energy fluence and several laser scans to precisely remove the thin films. If a single-scan, high energy fluence were used, then the machining reaches the silicon substrate, and the beam begins to thermally process the silicon. This leads to melting of the silicon, which quickly forms the recast layer as shown in Figure 5, especially at the end points where the laser deeply penetrates into the silicon substrate.

In the laser micromachining, the primary focus is to improve the quality of the cuts and it is important to ensure that the laser selectively ablates the material at the interaction site. When the material is vaporized, the particles are ejected in the forms of neutrals,

electrons, and ions. Because the electrons are much lighter than the electron, they are ejected before the ionic material, and quickly scatter due to the charges on the particles. If the pulse energy is high enough for the thermal regime, condensation may occur resulting in a recast layer around the edges of the machined feature. Melting causes the material to become fluid and redistributes it by the pressure created by the machining process. Recast layers are very difficult to remove because they are formed at very high temperature and rapidly solidified with strong bonding to the substrate. Ultrafast laser pulses are expected to eliminate this problem through ablation rather than melting, because the pulse duration is faster than the thermal diffusion time.

For bulk materials it is fairly easy to adjust the laser power density so that thermal damage can be minimized. However, multi-layer thin films may be composed of materials with different threshold energy values. If the laser energy is not high enough to ablate all the layers, then material removal might be incomplete. For this reason it is important that the laser energy be kept high enough to completely ablate all the layers in which it interacts. However, this high pulse energy also increases the minimum feature size in the thin films as well as melts the substrate. Alternatively, multi-pass surface micromachining at low energy fluence could be successfully applied to prevent the recast effects, however, this method leaves columnar structures in the bottom surface as shown in Figure 6.

Recast layers of the molten silicon are divided into low and high particle density (number of particles per unit volume) regions, both of which occur when deep trenches were machined into the silicon substrate. Low particle density region, characterized by something

like a suspension of sand particles embedded in a cotton ball (Figure 7), was observed along the edges of the channels and center of the finished device pattern (Figure 2). Such recast layers were weakly adhered to the surface and, because of the high surface area to volume ratio, this debris is easily removed by dipping in a KOH etchant.

This low particle density recast was present in all machined samples and is the result of the accumulation of condensing vapors of all machined materials. Figure 8 displays the high particle density recast layer, which could not be removed by chemical etching without damaging the deposited films. This type of debris appears to be the most challenging aspect of single pass surface micromachining. Future experiments should be carried out to eliminate this effect by etching the silicon out from behind the thin films with anisotropic KOH etchant, with subsequent machining done on the remaining films only.

Conclusions

Femtosecond laser surface micromachining of CVD-deposited polysilicon and PLD-deposited boride thin films on silicon substrate were performed. Single-scan laser micromachining yielded significant amount of recast layer due to high energy fluence that in turn melted the silicon substrate. Low energy fluence and multiple laser scans enabled an improvement in the quality and controlled the depth of channels. Because the energy fluence required for the silicon is so much higher than that of thin films, future experiments will include the machining of the films by wet etching the back of the wafer down to the silicon dioxide, the first of the thin films and an etch stop for KOH etchants. This will expose only

the materials that require low power densities as well as reduce the debris by allowing some of it to pass through the machined area.

References

[1] Micromachine Devices, "European Study Sees MEMS Market at More Than $34 Billion by '02," May, 1997, page 1

[2] Todd Lizotte, Terence O'Keeffe, and Justin Bruere: 11 Industrial Laser Review (1997)

[3] Resonetics, Inc, "Resonetics illustrated guide to laser applications micromachining," http://www.resonetics.com/applications.shtml

[4] Oxford Lasers, Inc., "Laser-based micromachining," http://www.oxfordlasers.com/MP.html

[5] Potomac technology, Inc., "Laser processing works on a micro scale," http://potomac-laser.com/technology/micro.html

[6] Hennink, S.C., "Machining lasers find niches by solving very small problems," Photonics Spectra, November,116-118,1997

[7] Shirk, M.D., and P.A. Molian, "A review of ultrashort pulsed laser ablation of materials," Journal of Laser Applications, V.10, No.1,1-11, 1998

[8] Liu, X., and G. Mourou, "Ultrashort laser pulses tackle precision machining," Laser Focus World, August, 101-118, 1997.

[9] Pronko, P., S. Dutta, J. Squier, J. Rudd, D. Du, and G. Mourou, "Machining of submicron holes using a femtosecond laser at 800 nm," Opt. Comm., V.114, 106-110, 1995

[10] Simon, P., and J. Ihlemann, "Machining of submicron structures on metals and semiconductors by ultrashort UV-laser pulses," Appl Phys A, 63, 505-508, 1996

[11] B. A. Cook, J. L. Harringa, T. L. Lewis, and A. M. Russell, Scripta mater. 42 (2000) 597

[12] A. M. Russell, B. A. Cook, J. L. Harringa, and T. L. Lewis, Scripta mater. 46 (2002) 629

[13] D. Emin, Physics Today, 31 (1987) 55

[14] H. Werheit, U. Kuhlmann, G. Krach, I. Higashi, T. Lundström, Y. Yu, J. Alloys Compounds, 202 (1993) 269

[15] B. A. Cook, J. L. Harringa, A. M. Russell, and S. A. Batzer, Machine Science and Technology, (under review)

[16] Marc Madou. Fundamentals of Microfabrication. Boca Raton: CRC Press, 1997

[17] R. Cherukuri, M. Womack, P. Molian, A. Russell, and Y. Tian, Surf. Coat. Technol. 155 (2002) 112

List of Figures

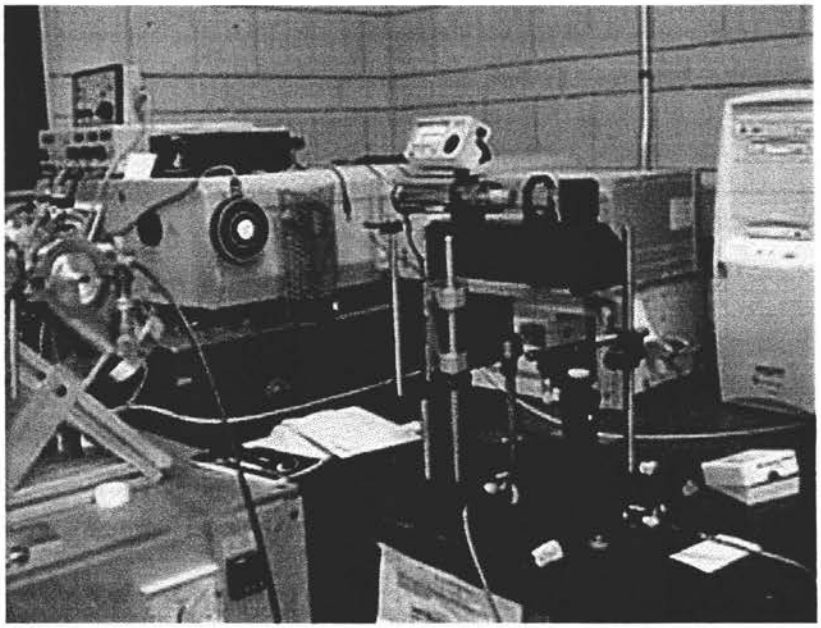

FIG. 1: FEMTOSECOND LASER AND FOCUSING SYSTEM

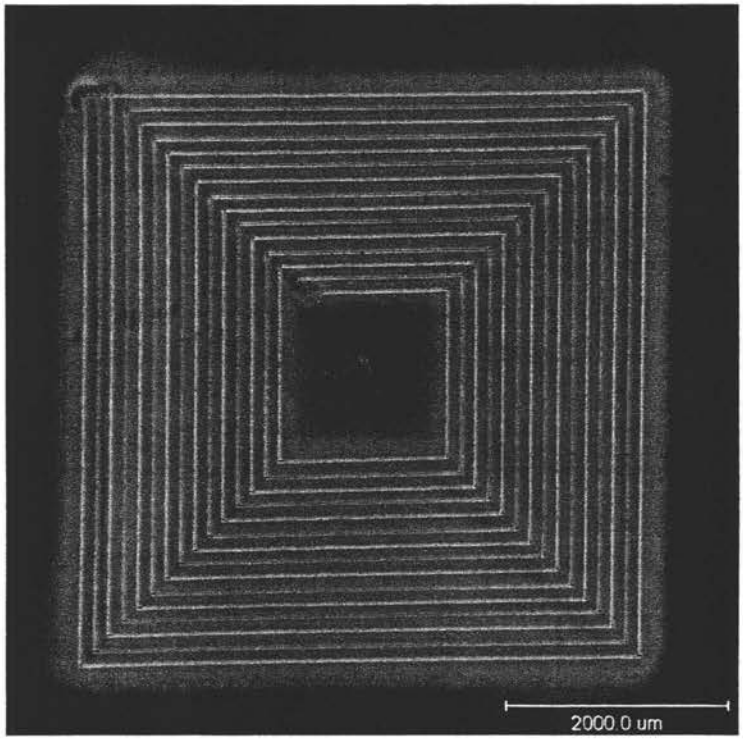

FIG 2: FABRICATED DEVICE

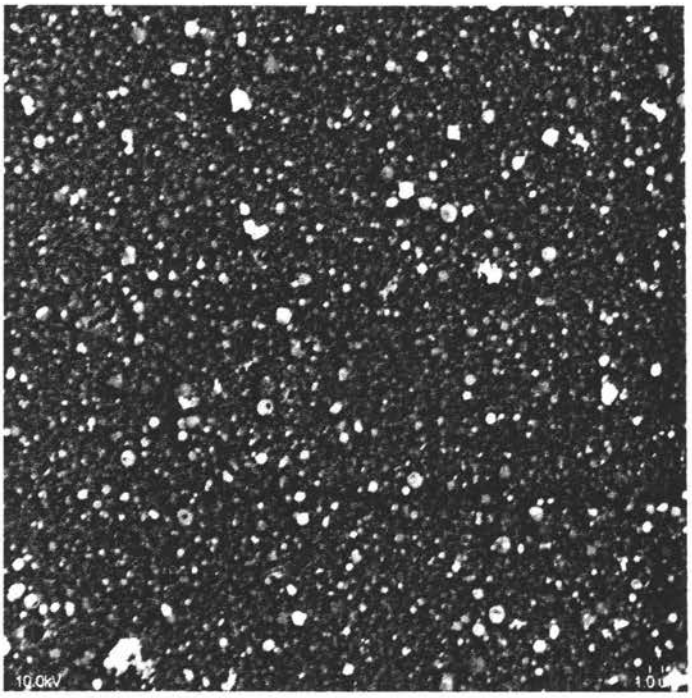

FIG 3: PLD-DEPOSITED BORIDE FILM

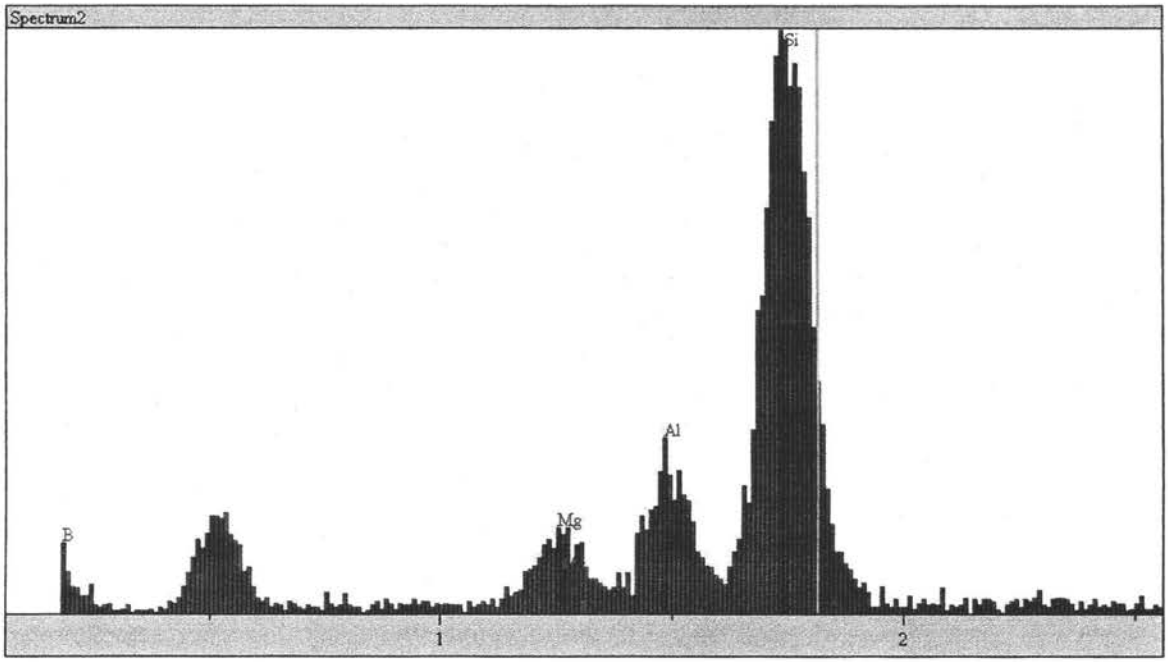

FIG 4: X-RAY SPECTROGRAPHOF DEPOSITED FILMS

FIG 5:RECAST LAYERS AROUND MACHINED REGIONS

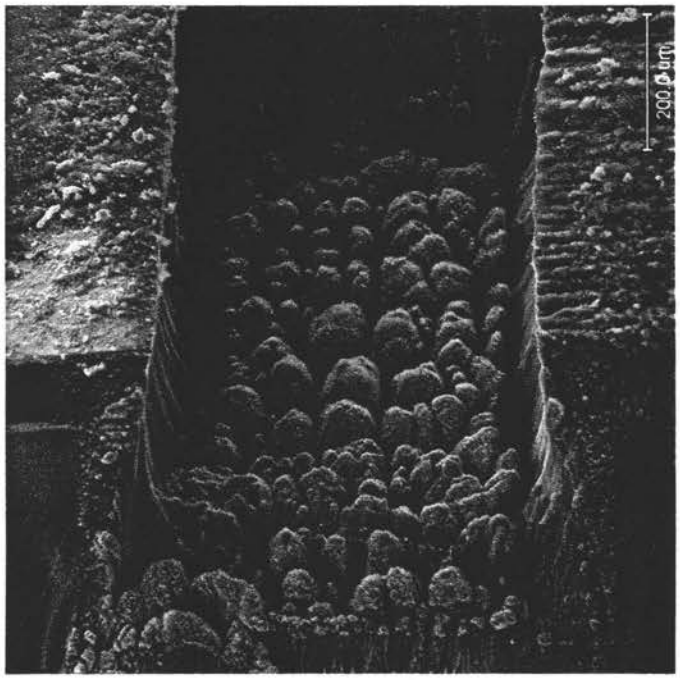

FIG 6: MULTIPASS MACHINED CHANNEL AT LOW ENERGY FLUENCE

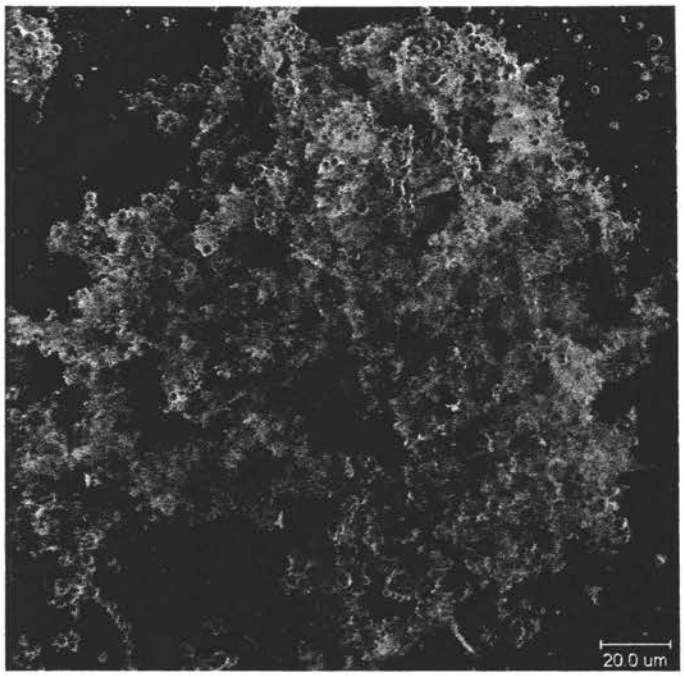

FIG 7: LOW PARTICLE DENSITY RECAST

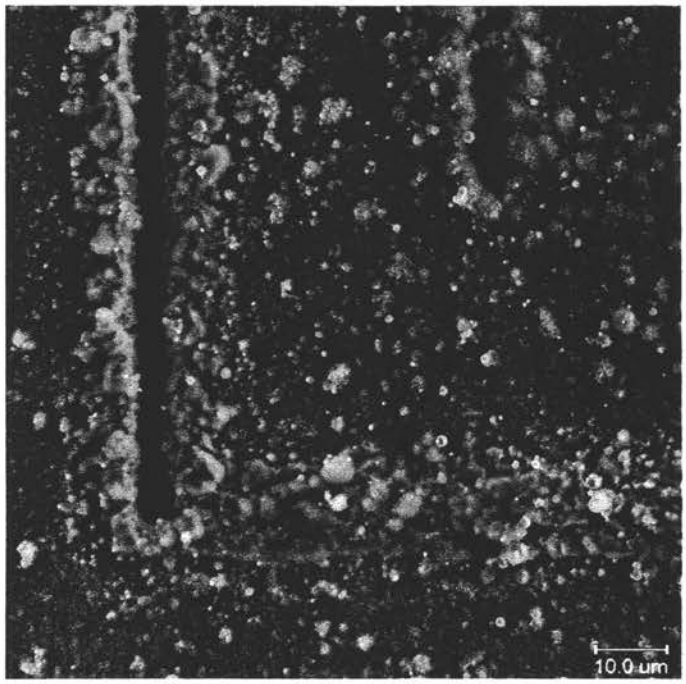

FIGURE 8: HIGH PARTICLE RECAST

CHAPTER 3. FEMTOSECOND PULSED LASER DEPOSITION OF ULTRA-HARD BORIDE THIN FILMS IN AMBIENT TEMPERATURE

A paper submitted to "Thin Solid Films" published by Elsevier Science S.A. Lausanne

Michael Stock, Allan Russell, and Pal Molian

Abstract

Thin films of ultra-hard $AlMgB_{14}$ were grown on Si (100) substrates at 300 K using femtosecond pulsed Ti:sapphire laser and subsequently annealed in argon gas up to 1373 K for two hours. X-ray photoelectron spectroscopy, X-ray diffraction, atomic force microscope, and nanoindentation were employed to study the composition, microstructure and hardness of thin films. Results were compared with nanosecond pulsed KrF excimer laser-deposited films. The as-deposited and post-annealed films (up to 1173 K), independent of the pulse width, exhibited amorphous structures with a hardness of 40 GPa. However, post-annealing at higher temperatures has varied effects on crystallization depending on the pulse width. The effect of pulse width on the microstructure and quality of thin films is discussed.

Introduction

The capability to synthesize *new* ultra-hard (> 40 GPa) and lubricant (coefficient of friction < 0.2) thin films has both immediate and long-term benefits for several applications such as cutting tools and MEMS. The need is severe because ultra-hard diamond thin films used presently are limited by the solubility of carbon in steels, silicon, and other carbide-forming alloys, while cubic BN thin films are hampered by poor adherence and impurities like hexagonal BN. A recent development in ultra-hard materials group is $AlMgB_{14}$

containing 0 to 30 mol% additives with a hardness in the range 32-46 GPa, where the highest hardness was observed in $AlMgB_{14}$ containing 30% TiB_2 [1]. A hardness of 45 GPa is comparable to the hardness of cubic-BN placing this material in the ultra-hard category. The nanocrystalline multiphase structure is said to be mainly responsible for its high hardness because single crystal $AlMgB_{14}$ has hardness of only 28 GPa [1]. Unlike the close-packed structures of diamond and cubic-BN, the crystal structure of $AlMgB_{14}$ is an open, body-centered orthorhombic, allowing incorporation of alloying elements such as Si and Ti B_2. Moreover, $AlMgB_{14}$ has higher electrical conductivity (~ 80 to 1500 $\Omega^{-1}m^{-1}$) and exhibits better thermal stability than many other hard materials [2].

Ultra-hard $AlMgB_{14}$ with its unique combination of mechanical, electrical and thermal properties is viewed as a material of high utility value similar to or better than other boron compounds such as B_4C, BN, TiB_2, and B_2O_3. $AlMgB_{14}$ is a promising candidate material for hard, wear-resistant and protective coating applications. In addition, $AlMgB_{14}$ is capable of serving as excellent self-lubricant by forming boric acid film through oxidation and reaction with ambient water vapor [3]. Boron compounds are prepared in the form of thin films by a variety of deposition methods: ECR microwave plasma assisted thermal evaporation [4], hot filament CVD [5], reactive RF magnetron sputtering [6, 7], pulsed DC magnetron sputtering [8], dual ion beam deposition [9], vacuum (cathodic) arc deposition [10], and pulsed laser deposition [11].

In this paper, we report the growth of thin films of $AlMgB_{14}$ by pulsed laser deposition (PLD) and examine the effect of pulse width on microstructure, film quality and

nanohardness. PLD was chosen because it is expected to reproduce the multicomponent $AlMgB_{14}$ target stoichiometry in the film by congruent ablation induced by the short pulse laser irradiation. We have also selected femtosecond (fs) PLD in this work not only for its technical merits but also for depositing films much faster than nanosecond (ns) PLD, making it more cost effective.

Pulsed Laser Deposition

PLD is about 20-year old technology with continuous development and offers significant potential for applications in microelectronics, hard coatings, and MEMS. It is a powerful yet simpler technique for growing thin films from the vapor phase. In PLD, an intense, short pulsed laser beam is focused onto a target material, resulting in emission of a plume of vaporized material (atoms, ions, neutrals, clusters, molten droplets, and particulates) and subsequent deposition on a substrate to grow the film [12-14]. Although there remain a number of unresolved scientific and technological issues, PLD is established as a commercially successful process for superconductor oxides such as $YBa_2Cu_3O_7$ due to its unique capability of faithful reproduction of the composition of the target [15, 16]. PLD is widely researched in university and R & D laboratories all over the world to deposit a variety of materials including magnetoresistant materials, semiconductors, ferroelectrics, polymers, and others [17-26].

Recent research in PLD is the use of high-intensity femtosecond pulsed lasers, which greatly modify the thermal processes in ablation due to the picosecond time scales of electron-electron thermalization and electron-phonon coupling [27-29]. As a result,

ultrashort laser pulses decrease the ablation threshold, reduce the amount of energy lost to plasma, increase the thermal gradients in the target as well as increase the vaporization over melting of the target. Some success stories of femtosecond PLD include: ablation of frozen acetone to deposit diamond-like carbon films on Si [30, 31]; growth of ZnO thin films on (0001) sapphire, quartz, and Si, with fewer droplets [32, 33]; deposition of thin films of TiN and BN on Si and BN/TiN superlattices [26]; growth of SnO_2 thin films on different sapphire surfaces [34, 35]; and homoepitaxy of Si(100) [36]. Most of these works confirm that the films deposited by the femtosecond pulsed lasers are superior than those deposited by the nanosecond pulsed lasers.

Experimental Details

$AlMgB_{14}$ films of about 100 nm in thickness were grown on thermally oxidized Si (100) substrates by a turbo-pumped vacuum PLD system. Two types of lasers were used as energy sources for ablation of hot-pressed $AlMgB_{14}$ target to generate the plasma plume in a high vacuum chamber (base pressure ~ 5×10^{-7} Torr). One was a Ti:sapphire laser (λ 800 nm, pulse energy 0.1 mJ, pulse duration 120 fs, repetition rate 1 kHz, spot size 150 μm round) and the other was a KrF excimer laser (λ 248 nm, pulse energy 70 mJ, pulse duration 20 ns, repetition rate 10 Hz, spot size 1 mm x 0.5 mm rectangle). The target had some oxygen impurity in the form of $MgAl_2O_4$ spinel phase. It also contained Fe and C impurities formed through the wear debris during the preparation of boride target in high-energy steel ball mill [1]. The substrate was placed parallel to the target at a distance of 40 mm. The deposition was carried out at room temperature (300 K) for about 30 to 60 minutes.

After deposition, the films were annealed at 1073 K to 1373 K at the intervals of 100 K for two hours, the annealing process was conducted in NRC 2940 high temperature vacuum furnace, which was evacuated below 2×10^{-6} Torr and then backfilled with yttrium gettered Ar to ambient pressure. The temperature ramp rate was set at 17°C/min. X-ray diffraction (XRD) patterns of the films were collected using a Scintag θ-2θ x-ray diffractometer with Cu K_α radiation. Surface topography and roughness of the films were studied using a Digital Instruments Dimension 3100 atomic force microscope (AFM) operated in tapping mode with a silicon pyramidal probe. The film thickness was measured by AFM. X-ray photoelectron spectroscopy (PHI™ Physical Electronics 5500 Multitechnique ESCA system) with monochromatic Al K_α radiation (1486.6 eV) and standard Mg/Al sources was used to determine the compositional information of the films. The Au $4f_{7/2}$ and Cu $2p_{3/2}$ excitations at 84.0 eV and 932.6 eV were used for energy calibration, and the atomic concentration was calculated by using the sensitivity factors provided with the PHI™ acquisition software. The base pressure for the analyzer system was less than 3×10^{-10} Torr. The films were subjected to an Ar^+ ion bombardment using 4 kV Ar^+ ions at 3 μA total target current to remove the surface oxide layer prior to the XPS analysis.

Results and Discussion

Table 1 shows the atomic concentration of as-deposited $AlMgB_{14}$ films for both lasers. It can be seen that the atomic ratio of Al, Mg and B for ns-laser films is very close to 1:1:14 stoichiometry with ~ 2 at.% excess Al. Oxygen content in the film is higher than normally expected for chamber base pressure attained in this work (~ 5×10^{-7} Torr), which

may be due to the $MgAl_2O_4$ content of the $AlMgB_{14}$ target. However, in contrast to ns-laser film, the atomic ratio of Al, Mg and B for fs-laser films deposited at room temperature deviates greatly from 1:1:14 stoichiometry with significant B deficiency. In addition, the oxygen and carbon concentrations were abnormally higher. The difficulty in reproducing the stochiometry of Al-Mg-B system by the fs-laser is attributed to one or more of the following reasons: 1) the femtosecond laser ablation due to its extreme intensity generates much higher-energy, higher-velocity particles (ionized and excited species) from the coupling of a large optical field with the solid target. Consequently, the high kinetic energy species tend to sputter the film during deposition; 2) the pulse energy is absorbed to a smaller depth of the target in fs-laser than ns-laser ablation (due to multiphoton absorption mechanism) such that the average composition of ablated species would not correspond to that of the target; and 3) the impurities such as oxides strongly absorb the 800 nm wavelength of femtosecond laser, evaporate and condense on the film, reducing the effectiveness of *congruent ablation.*

Figure 1 shows the XRD patterns of fs-laser deposited and 1273 K post-annealed $AlMgB_{14}$ films. Thin film XRD setup was used here to prevent the reflections from the silicon substrate. No diffraction peaks characteristic of crystalline structures can be seen, suggesting that the structure is amorphous. The formation of amorphous structure is partly attributed to the low substrate temperatures, where there is not enough time for *adatoms*, due to limited surface mobility, to find positions of energy minima before being constrained by subsequently deposited atoms. Thus these atoms are "quenched" onto the substrate surface, facilitating the formation of non-equilibrium amorphous structure.

Figure 1 also shows that the amorphous structure was stable in post-annealing up to 1273 K. However, post-annealing at 1373 K caused the film to complete crystallization (Figure 2) although no reflection peaks corresponding to $AlMgB_{14}$ were identified. There are two strong peaks at $2\theta=17.27^{\circ}$ and $2\theta=53.52^{\circ}$ both of which match with the reflections of SiB_6. It is believed that the presence of impurities such as carbon and oxygen in the film and absence of stochiometry inhibited the crystallization to $AlMgB_{14}$. For example, the C impurity was reported to promote the formation of β-AlB_{12} phase in preference to $AlMgB_{14}$ [37]. The presence of a large amount of oxygen in the fs-deposited film might be able to further inhibit the formation of crystalline $AlMgB_{14}$ phase because the oxidation of Al, Mg and B was more energetically favorable, yielding a complex oxide glass structure with B playing the role of network former [38].

Thermodynamics and kinetics strongly favor the formation of SiB_6 at 1373 K by the high-temperature diffusion of Si from substrate through oxide layer into the interior of the film. This also shows the failure of the amorphous SiO_2 layer as a diffusion barrier at this temperature. The various defects, such as vacancies, pinholes, and microporosity, etc., (formed in the as-deposited film as a result of room temperature deposition) are believed to provide an effective pathway for faster Si diffusion.

Figure 3 shows the XRD patterns of ns-laser deposited films. Here we have used standard powder XRD monochromator to obtain the patterns. Aside from the Si (200) reflection centered at $2\theta \sim 33^{\circ}$, the XRD pattern for as-deposited film did not exhibit diffraction features charateristic of crystalline structures. Although the Si (200) is a

"forbidden" peak, it can appear because of growth-induced compressive stress leading to a slight distortion of the Si unit cell from cubic to tetragonal. The as-deposited and annealed films up to 1173 K showed amorphous structures similar to fs-films. However, the XRD pattern for 1273 K annealed film showed four sharp diffraction peaks, illustrating the full crystallization of the amorphous phase. Three peaks centered at 2θ positions of 13.85°, 27.89° and 42.37° were identified to correspond to (011), (022) and (033) planes of the $AlMgB_{14}$ orthorhombic structure respectively. Obviously, a strong (011) crystallographic texture has developed because the high adatom energy achieved in PLD can lead to the formation of such preferential orientation. It should be noted that the intensity ratio of the (022) peak to the (033) peak, $I_{(022)}/I_{(033)}$, is approximately 1:3 and agrees well with the standard $AlMgB_{14}$ powder diffraction pattern, whereas the intensity of the (011) peak relative to that of the (022) and (033) peaks appears to be abnormally faint, which is thought to be a consequence of the special low-angle diffraction geometry for a small, thin film sample. The small peak centered at $2\theta = 17.27°$ can be ascribed to SiB_6.

The quality of fs-laser films was much better than those of ns-laser films. The films deposited by the fs-laser exhibited fewer particulates, smoother surfaces, and no cracks. Figure 4 shows the AFM images of 1273 K annealed ns- and fs-laser film surfaces. For ns-laser film surface, many surface cracks were found and attributed to the thermal shrinkage occurring during the crystallization process. Islands of cracks with lateral size ranging from about 200 nm to 800 nm were observed in the annealed film. Because the thermal expansion coefficient of the Si substrate ($\sim 4 \times 10^{-6}$/K) is much less than that of crystalline $AlMgB_{14}$ film ($\sim 9 \times 10^{-6}$/K) [39], a significant tensile stress was built up during the cooling and

initiated the cracks. In addition, the particulate density was much lower for the fs laser films compared to ns laser films, a feature well supported in the literature [40].

Conclusions

Ultra-hard, amorphous thin films of $AlMgB_{14}$ were grown on Si substrates by nanosecond and femtosecond PLD methods. Unlike that of ns-laser films, the stochiometry of fs-laser films deviated largely from the target due to the sputtering of the film by high kinetic energy species emission, large absorption coefficient, and impurity (C, O) deposition. The polycrystalline orthorhombic $AlMgB_{14}$ phase, accompanied by the development of pronounced (011) preferred orientation, was observed only in the post-annealed, ns-laser films. In contrast, crystalline SiB_6 was formed in post-annealed fs-laser films at 1373 K due to the favorable high-temperature diffusion. The film quality of ns-laser films in terms of cracking, particulate formation, and surface roughness was much inferior to those of the fs-laser films.

Acknowledgements

The authors sincerely acknowledge the financial support provided by the National Science Foundation under grant DMI-0084969 for this work. The authors also wish to express their appreciation to Yun Tian of Iowa State University and Balu Balachandran of Argonne National Laboratory for helping in AFM, XPS, and XRD.

References

[1] B. A. Cook, J. L. Harringa, T. L. Lewis, and A. M. Russell, Scripta Mater. 42 (2000) 597.

[2] B. A. Cook, J. L. Harringa, T. L. Lewis, Y. B. Lee, and A. M. Russell, J. Adv. Mater. (in press)

[3] A. Erdemir, G. R. Fenske, and R. A. Erck, Surface Coatings and Technology, 43/44 (1990) 588.

[4] S. M. Gorbatkin, R. L. Rhoades, T. Y. Tsui, and W. C. Oliver, Appl. Phys. Lett. 65 (1994) 2672.

[5] S. V. Deshpande, E. Gulari, S. J. Harris, A. M. Weiner, Appl. Phys. Lett. 65 (1994) 1757.

[6] C. Doughty, S. M. Gorbatkin, T. Y. Tsui, G. M. Pharr, D. L. Medlin, J. Vac. Sci. Technol. A 15, (1997) 2623.

[7] D. Music, J. M. Schneider, V. Kugler, S. Nakao, P. Jin, M. Östblom, L. Hultman, and U. Helmersson, J. Vac. Sci. Technol. A 20 (2002) 335.

[8] M. U. Guruz, V. P. Dravid, Y. W. Chung, Thin Solid Films 414 (2002) 129.

[9] K. F. Chan, C. W. Ong, C. L. Choy, R. W. M. Kwok, J. Vac. Sci. Technol. A 17 (1999) 2944.

[10] C. C. Klepper, R. C. Hazelton, E. J. Yadlowsky, E. P. Carlson, M. D. Keitz, J. M. Williams, R. A. Zuhr, and D. B. Poker, J. Vac. Sci. Technol. A 20 (2002) 725.

[11] F. Kokai, M. Taniwaki, K. Takahashi, A. Goto, M. Ishihara, K. Yamamoto, Y. Koga, Diamond Relat. Mater. 10 (2001) 1412.

[12] P. R. Willmott and J. R. Huber, Rev. Modern Phys. 72 (2000) 315.

[13] K. L. Saenger, Proc. Adv. Mat. 2 (1993) 1.

[14] D. B. Chrisey and G. K. Hubler, Pulsed Laser Deposition of Thin Films, Wiley, New York, 1994.

[15] C-S. Kim, S. C. Song, and S. Yeol Lee, Appl. Surf. Sci. 168 (2000) 316.

[16] J. Schubert, M. Siegert, M. Fardmanesh, W. Zander, M. Prömpers, Ch. Buchal, J. Lisoni, and C. H. Lei, Appl. Surf. Sci. 168, (2000) 208.

[17] A. Venimadhav, M. S. Hegde, R. Rawat, I. Das and M. El Marssi, J. Alloys and Compounds 326 (2001) 270.

[18] J. -M. Liu, Q. Huang, J. Li, C. K. Ong, X. Y. Chen, Z. G. Liu and Y. W. Du, Mat. Lett. 50, (2001) 97.

[19] J. Ohta, H. Fujioka, H. Takahashi, M. Sumiya and M. Oshima, J. Crystal Growth 233 (2001) 779.

[20] M. Cazzanelli, D. Cole, J. Versluijs, J. F. Donegan and J. G. Lunney, Mat. Sci. Eng. B 59 (1999) 89.

[21] C. M. Rouleau and D. H. Lowndes, Appl. Surf. Sci. 127- 129 (1998) 418.

[22] L. Goux, M. Gervais, F. Gervais, C. Champeaux and A. Catherinot, Int. J. Inorg. Mat. 3 (2001) 839.

[23] C. H. Hur, K. B. Han, K. A. Jeon and S. Y. Lee, Thin Solid Films, 400 (2001) 169.

[24] H. Sankur, W. J. Gunning, J. DeNatale, and J. F. Flintoff, J. Appl. Phys. 65 (1989) 2475.

[25] Y. Yue, Y. K. Ho, Z. Y. Pan, R. W. Lee, Z. Y. Man, and J. Xie, Phys. Lett. A 235 (1997) 267.

[26] Z. Zhang, P. A. VanRompay, J. A. Nees, R. Clarke, X. Pan, P. P. Pronko, Appl. Surf. Sci. 154- 155 (2000) 165.

[27] P. P. Pronko, S. K. Dutta, D. Du, and R. K. Singh, J. Appl. Phys. 78 (1995) 6233.

[28] P. P. Pronko, P. A. Van Rompay, and S. Sato, Proc. SPIE- Intrational Society for Optical Engineering, Vol. 3269 (1998) 46.

[29] P. P. Pronko, Z. Zhang, and P. A. VanRompay, Appl. Surf. Sci. 9643 (2003) 1.

[30] M. Okoshi, S. Higuchi, and M. Hanabusa, J. Appl. Phys. 86 (1999) 1768.

[31] M. Okoshi, S. Higuchi, M. Hanabusa, Appl. Surf. Sci. 145- 155 (2000) 376.

[32] E. Millon, O. Albert, J. C. Loulergue, J. Etchepare, D. Hulin, W. Seiler, J. Perrière, J. Appl. Phys. 88, (2000) 6937.

[33] M. Okoshi, K. Higashikawa, M. Hanabusa, Appl. Surf. Sci. 145-155 (2000) 424.

[34] J. E. Dominguez, L. Fu, X. Q. Pan, Appl. Phys. Lett. 79 (2001) 614.

[35] J. E. Dominguez, X. Q. Pan, L. Fu, P. A. Van Rompay, Z. Zhang, J. A. Nees, and P. P. Pronko,, J. Appl. Phys. 91 (2002) 1060.

[36] M. Hegazy and H. Elsayed-Ali, J. Vac. Sci. Tech. A, 20 (2002) 2068.

[37] H. Werheit, U. Kuhlmann, G. Krach, I. Higashi, T. Lundström, Y. Yu, J. Alloys Compd. 202 (1993) 269.

[38] Y. Tian, M. Womack, P. Molian, C. C. H. Lo, J. W. Anderegg, A. M. Russell, Thin Solid Films 418 (2002) 129.

[39] A. M. Russell, B. A. Cook, J. L. Harringa, T. L. Lewis, Scripta Mater. 46 (2002) 629.

[40] F. Qian, R. K. Singh, S. K. Dutta, and P. P. Pronko, Appl. Phys. Lett. 67 (1995)3120.

List of Tables

TABLE I. Atomic composition of as-deposited thin films

Laser	B	Al	Mg	O	Fe	C
Nanosecond	71.46	7.41	4.98	9.53	4.67	1.95
Femtosecond	49.25	5.06	5.80	24.90	2.89	11.88

List of Figures

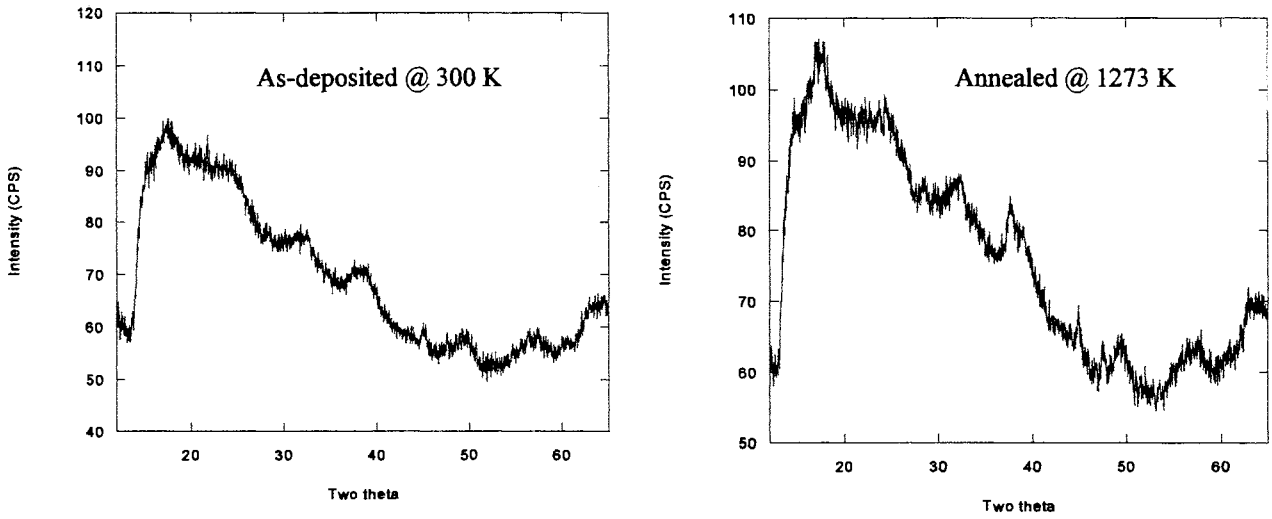

(a) (b)

FIG.1. XRD patterns of femtosecond pulse-laser deposited thin films of $AlMgB_{14}$ (a) as-deposited film (b) post-annealed at 1273 K

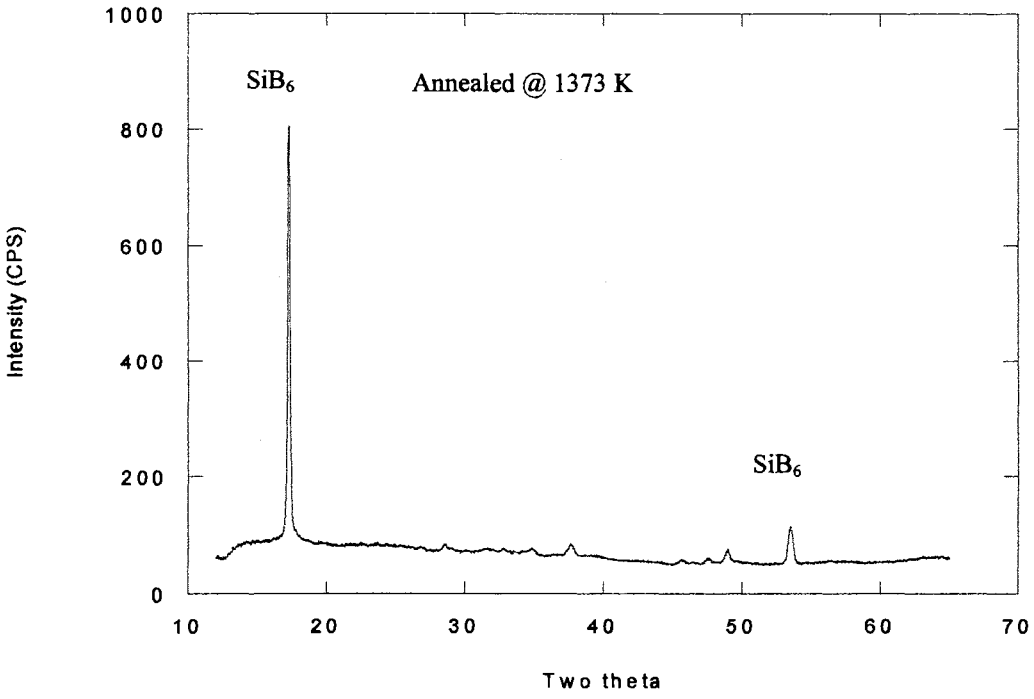

FIG.2. XRD pattern of femtosecond pulse-laser deposited and 1373 K annealed films

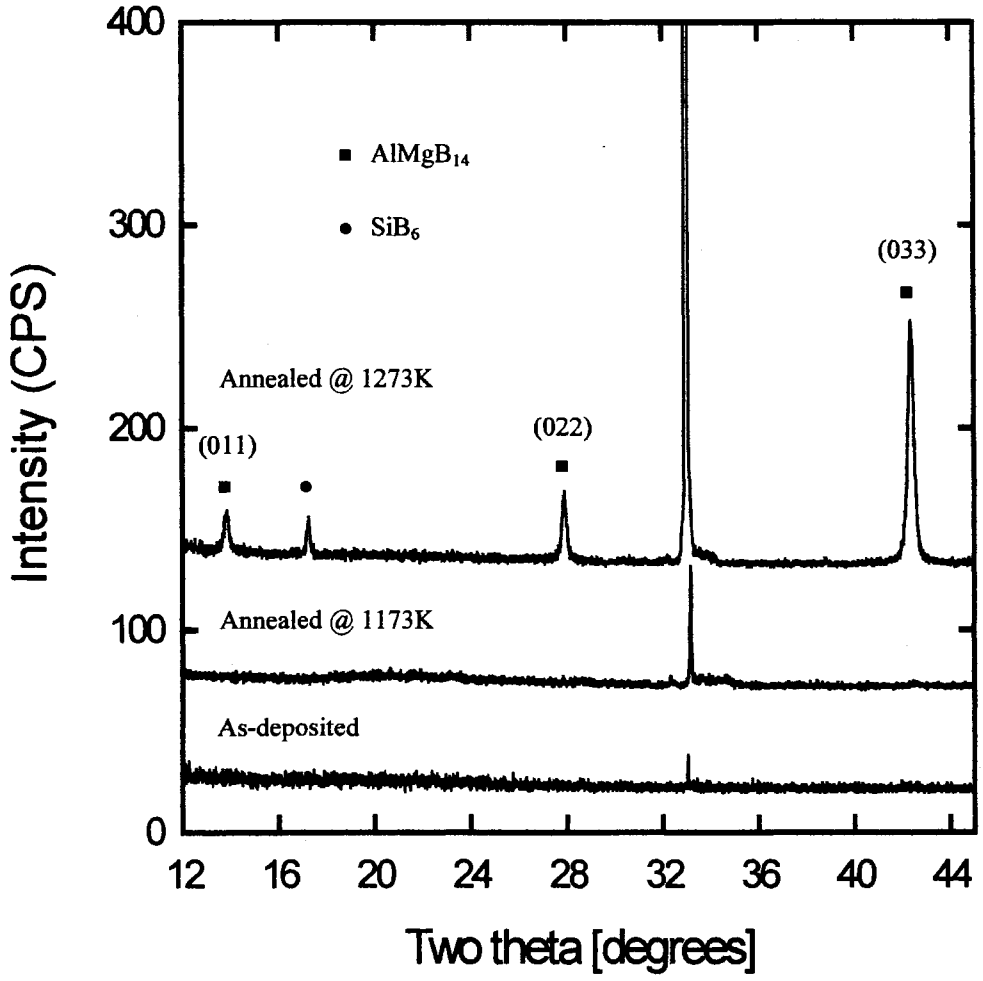

FIG. 3. XRD patterns of nanosecond pulse-laser deposited $AlMgB_{14}$ films

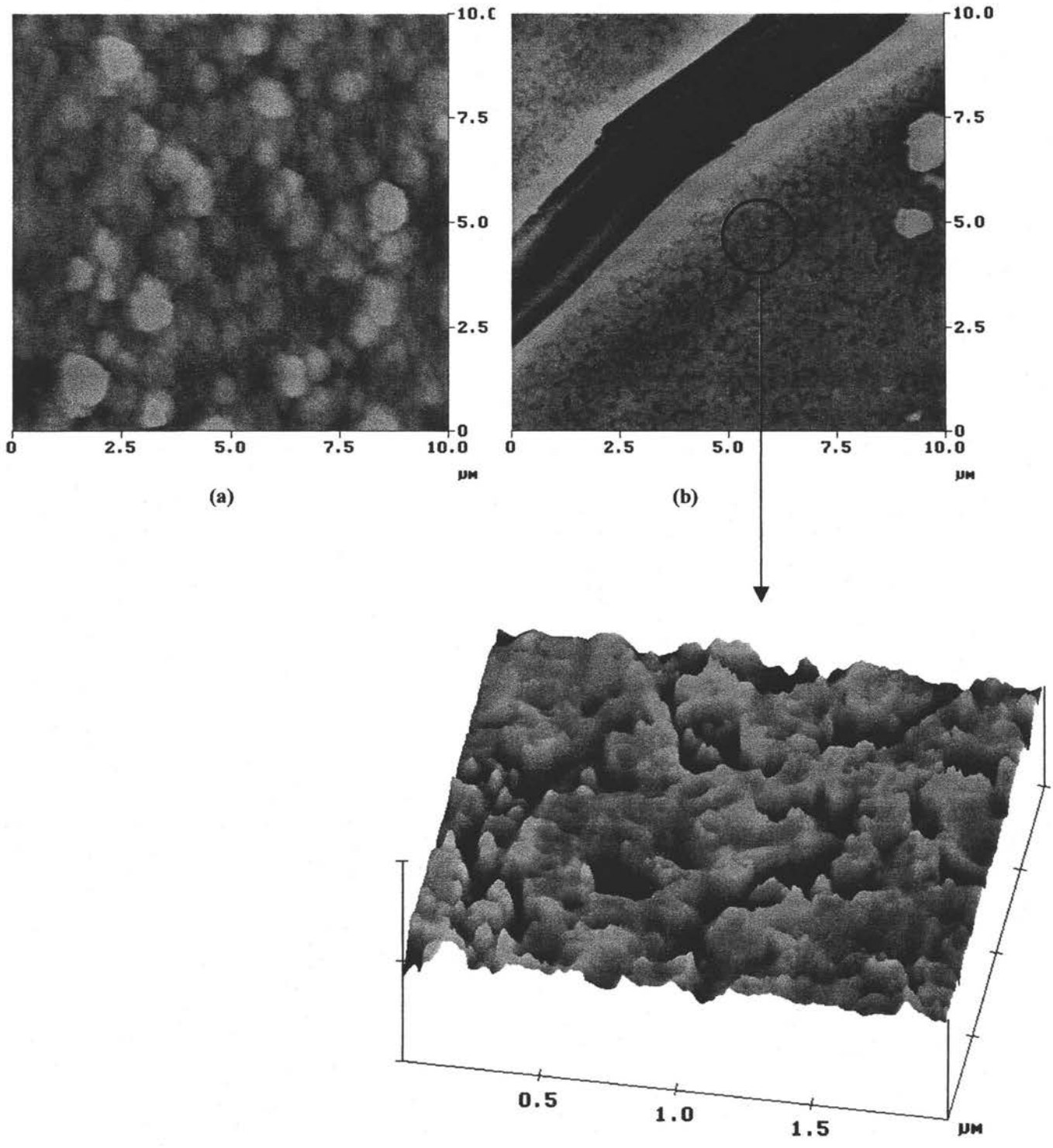

FIG. 4. AFM images of laser grown and post-annealed (1273 K) $AlMgB_{14}$ film surfaces (a) fs-PLD (b) ns-PLD

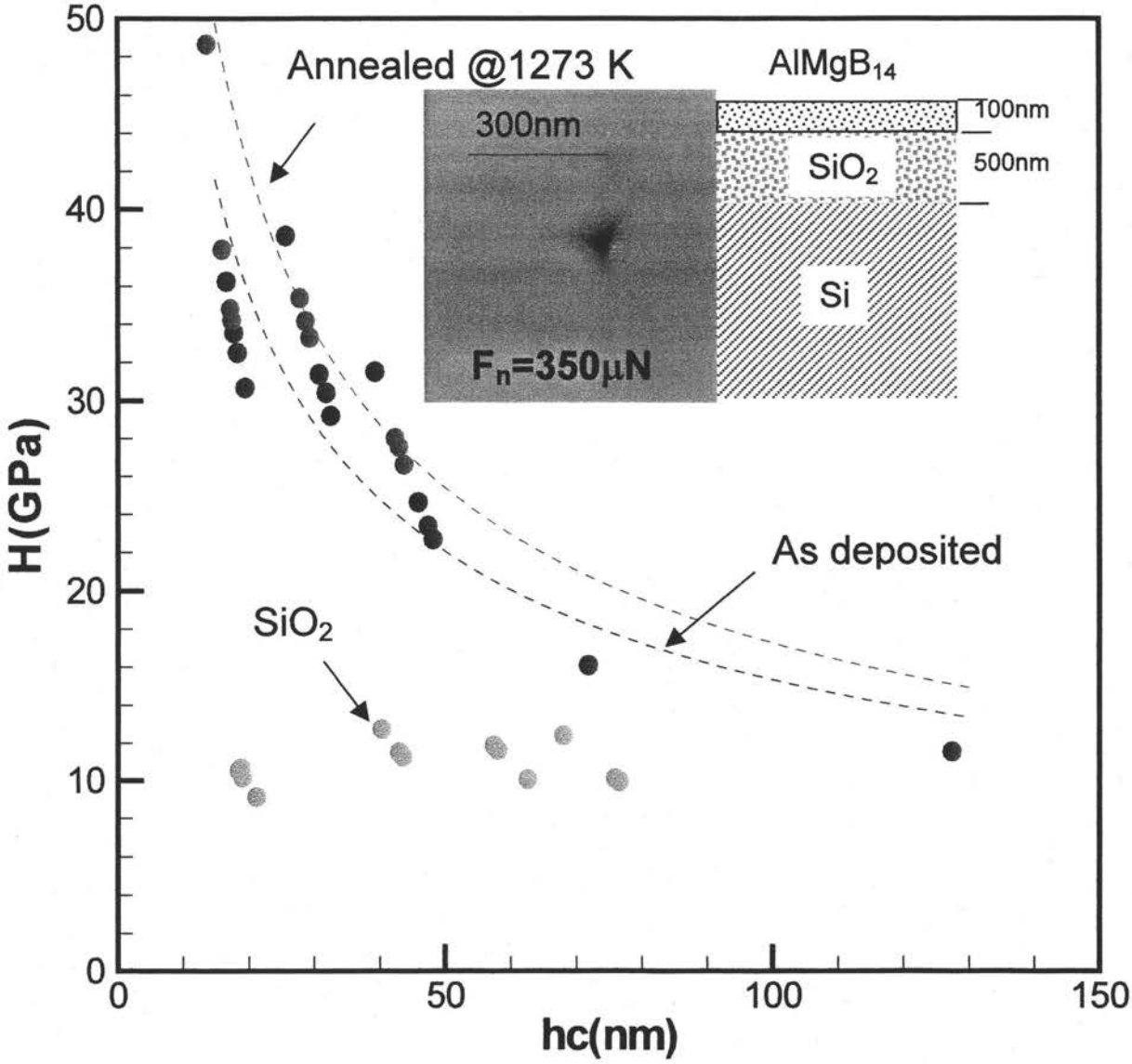

FIG.5. Nanoindentation hardness of $AlMgB_{14}$ thin film as a function of depth (nanosecond pulsed laser)

CHAPTER 4. EFFECTS OF POLARIZATION ON SURFACE MICROMACHINING

Introduction

The quality of the features produced by the laser micromachining is determined by many factors such as energy distribution, mode, beam aberration, pulse duration, beam polarization, and material/beam coupling properties to name a few. Of this list polarization is unique because its effects are non-isotropic. In this section, we explore the effects of polarization on the resulting surface quality of the features produced by laser micromachining.

While the electric and magnetic fields have different polarization properties in general, polarization usually refers to the electric field of the electromagnetic wave [1]. The beam is classified by the direction in which the electric field oscillates; vertical, horizontal, or circular. As discussed in Chapter 1, both horizontally and circularly polarized beams were used to laser micromachine the features of a MEMS device, which produced asymmetric and approximately symmetric results respectively. These results are explored further in this section and related to the equations that govern the propagation of the beam.

Models for Wave Propagation

The electromagnetic wave is composed of two simultaneously propagating electric **E** and magnetic **B** waves that are oriented perpendicularly to each other at an angular frequency ω. [1]

$$E(r,t) = \mathrm{Re}\{E(r)e^{-i\omega t}\} = E_r(r)\cos\omega t + E_i(r)\sin\omega t$$
$$B(r,t) = \mathrm{Re}\{B(r)e^{-i\omega t}\} = B_r(r)\cos\omega t + B_i(r)\sin\omega t \quad (3)$$

The amplitude vector of a circularly polarized beam rotates about the axis of propagation with a frequency equal to that of the wave.

The real vectors of the electric field can be specified when $\mathbf{E_1}$ and $\mathbf{E_2}$ perpendicular so that their orthogonal components are:

$$\begin{pmatrix} E_1^2 \\ E_2^2 \end{pmatrix} = \frac{1}{2}\left[E_r^2 + E_i^2 \pm \sqrt{(E_r^2 - E_i^2)^2 + 4(\boldsymbol{E}_r \cdot \boldsymbol{E}_i)^2}\right] \quad (2)$$

For linear polarization (horizontal or vertical) $\mathbf{E_2}$ is zero and the real and imaginary parts of the wave are collinear. For circular polarization the real and imaginary parts are equal and perpendicular, therefore $\mathbf{E_r}^2=\mathbf{E_i}^2$ [1]. This is clearly a simplified model of the complex wave propagation, but will be sufficient to understand the effects of polarization on the features that are machined. This basic model can be shown to produce a graph of the electric field in the focal plane at time zero for a circularly polarized beam shown in Figure 1. As seen, the polarity of the beam varies from circular to linear as the distance from the propagation axis increases, and is only truly circularly polarized in the center of the beam where the direction of the vector rotates about this axis.

The fact that linearly polarized beams produce features that will be deeper when the control stage is moving in the p direction than the s direction as seen in Figure 2, causes the edges of even a circularly polarized beam to exhibit similar asymmetric behavior seen in

Figure 3. The walls of the feature are clearly slanted in when machining is done in the horizontal direction, due to the ineffective machining characteristics of the perimeter of the beam, and perpendicular to the surface in the vertical direction. Both channels appear to be equal in depth and quality in the center of the machined channel, demonstrating the presence of circular polarization at the center of the beam. This is especially apparent when compared to features in Figure 2.

Laser-Matter Interaction

For femtosecond laser pulses a two phase model is generally used to describe the material removal process. This model assumes that the electrons within an optical skin depth absorb the pulse energy so rapidly that electron lattice interaction is limited. This leads to a thin layer of plasma that is hydrodynamically stable during irradiation[2]. However, absorption of the pulse results in energy relaxation within the electron subsystem, thermal diffusion, and energy transfer by electron-phonon coupling to the lattice [4]. At this point the addition of more energy is compensated by an increase in energy transfer to the lattice because the heat capacity of the electron system remains constant. A two phase model assumes that the phase transition and plasma do not effect the substrate material. Femtosecond pulses minimize the amount of energy that is transferred from the electrons to ions when compared to nanosecond pulses. This is favorable because this type of energy transfer involves a much larger volume than the focus volume, which results in a breakdown of the two phase model by producing a liquid phase which is violently ejected from the machined feature [3].

When the pulse energy is high the heat effects of the pulse penetrates the material more deeply because of the transfer of excess energy in the plasma cloud and the target material as seen in Figure 4 [2]. Also the electron temperature gradient is lower which produces a relatively large region in which a liquid phase is possible. With lower energy pulses the temperature gradient is very high which more closely produces results consistent with the two phase model because only the material within the optical depth, which is directly and intensely irradiated, is effected. In this situation the electron temperature is either very high, producing ionization, or very low, which causes little physical change in the material.

Conclusion

While circularly polarizing a beam that is to be used to micromachine a multi dimensional feature does improve the feature quality, it should be noted that differences will exist at the edges of single pass channels due to the polarity profile that exists in focused beams. The effects are minimized when a multi-pass approach is employed during machining.

The physical effects of excess energy absorption can be seen in the sequence of single pass lines machined at varying energies. Clearly it can be seen that as the pulse energy is increased from Figure 5a to 5d, the amount of ejected recast increases greatly. Experimental data should be used to determine the appropriate energy levels used in multi-layer micromachining.

References

[1] Leckner, John., "Polarization of tightly focused laser beams," J. Opt. A: Pure Appl. Opt. 5 (January 2003) 6-14

[2] Zhang, Ying., Zhang, Jie., Pan, Shao-hua., Nie, Yu-xin., "A simple model for electron temperature and penetration depth in interaction of ultra-short laser pulses with solid targets," J. Physics. D: Appl Phys. 30 (1997) 655-660

[3] Ramanathan, Diwakar., Molian, Pal A., "Micro- and Sub-Micromachining of Type Iia Single Crystal Diamond Using a Ti:Sapphire Femtosecond Laser," Journal of Manufacturing Science and Engineering: May 2002, Vol.124

[4] Nolte, S., Momma, C., Jacobs, H., Tunnermann, A., "Abalation of metals by ultrashort laser pulses," J. Opt. Soc. Am. B/Vol. 14, No. 10/ October 1997

List of Figures

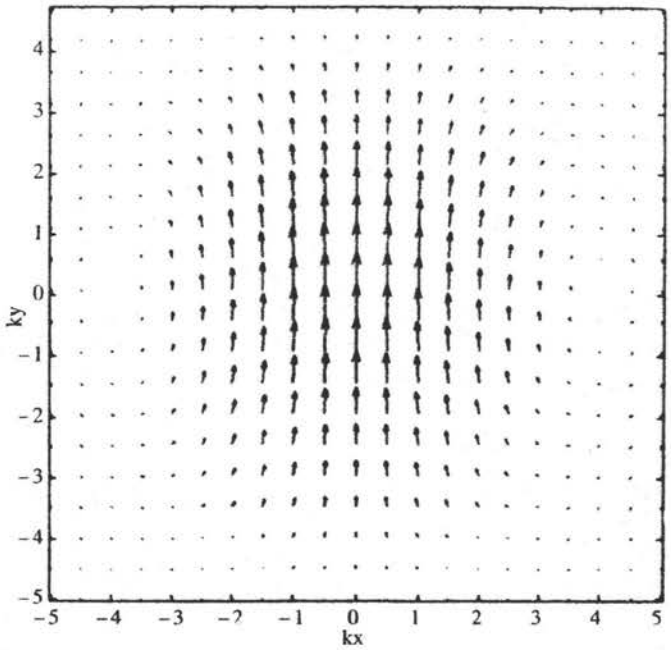

FIG 1: Electric field of a circularly polarized beam at the focal plane

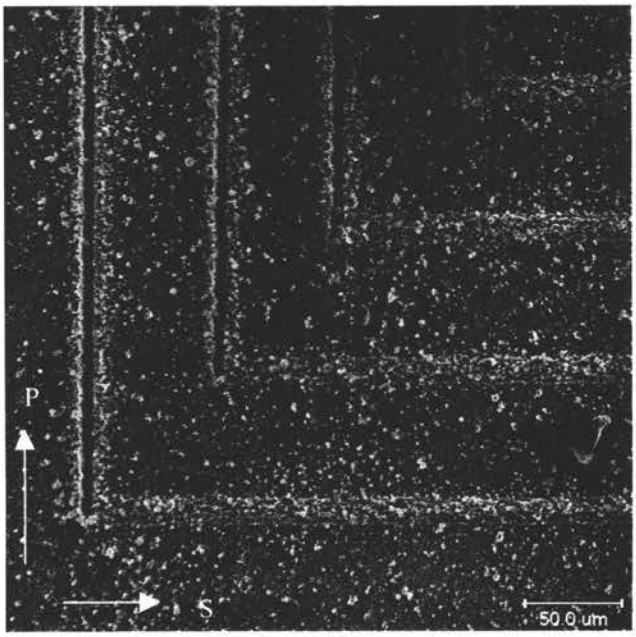

FIG 2: Asymmetric features produced by a horizontally polarized beam

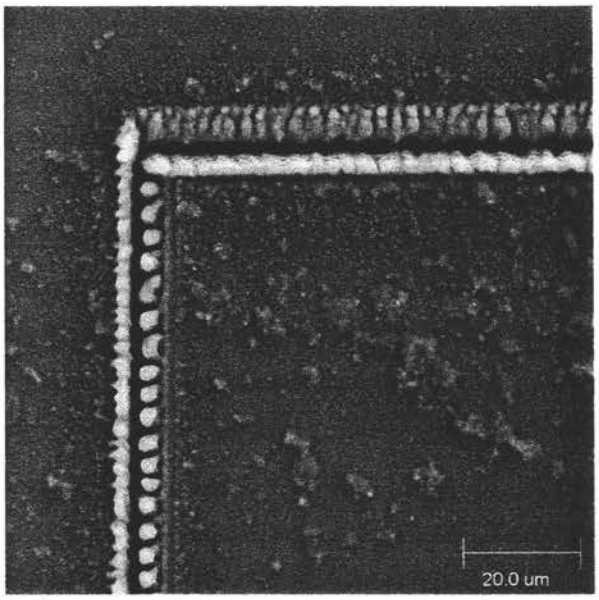

FIG 3: Features with asymmetric edges produced by a circularly polarized beam

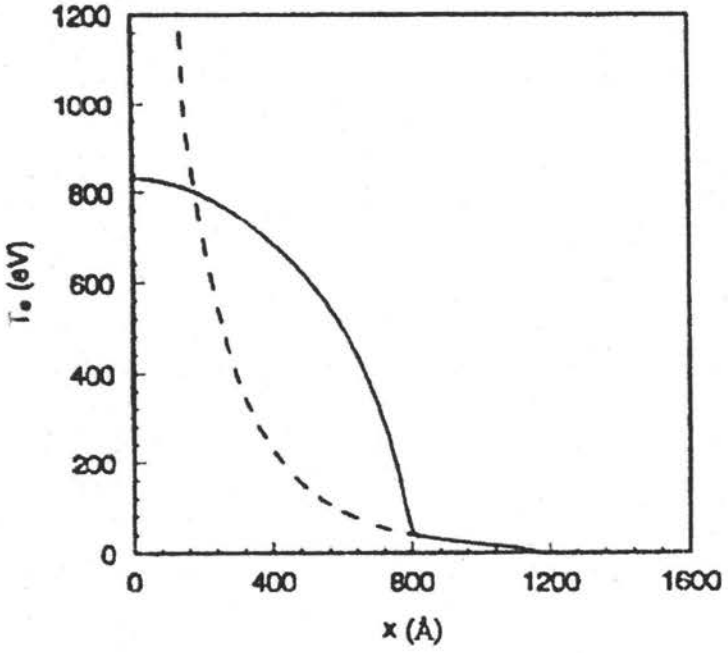

FIG 4: Electron temperature verses depth including electron conduction (solid) and femtosecond irradiation only (dashed line)

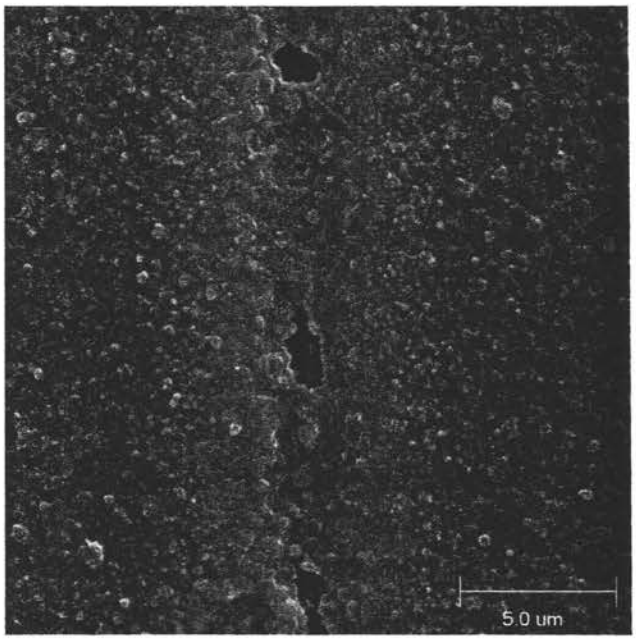

FIG 5a: Channel machined at .3μJ

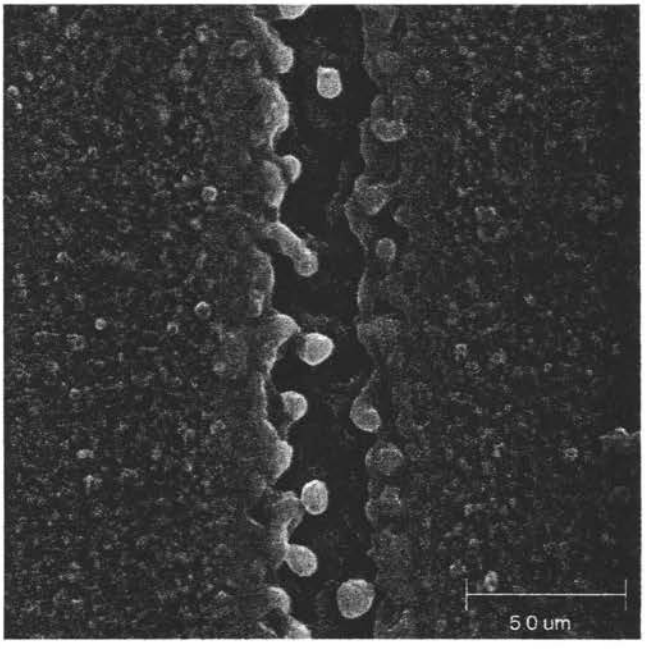

FIG 5b: Channel machined at .5 μJ

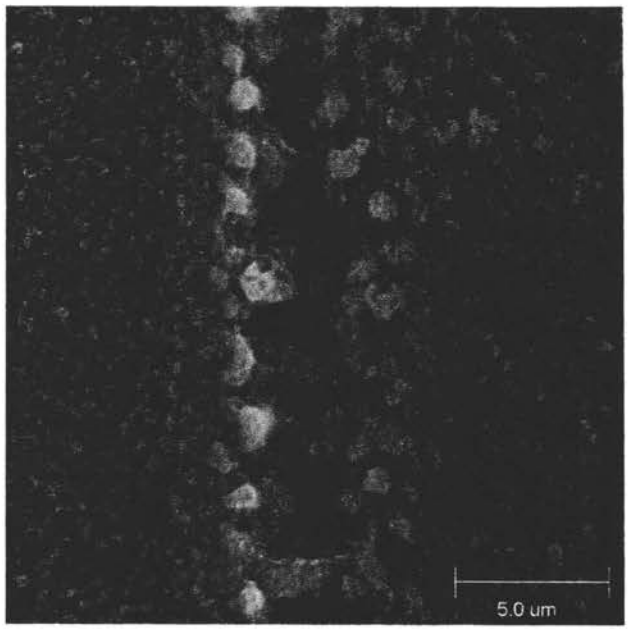

FIG 5c: Channel machined at 1 μJ

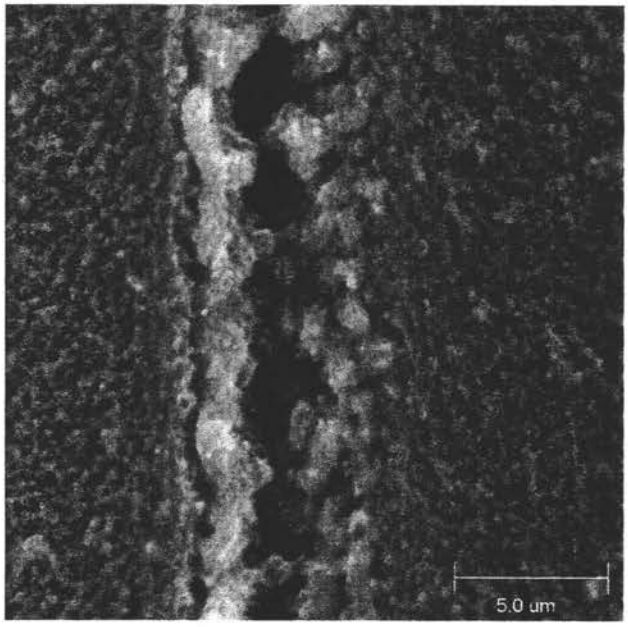

FIG 5d: Channel machined at 3 μJ

CHAPTER 5: GENERAL CONCLUSIONS AND CONCEPT REVIEW

Concept Review

We have presented some of the major influences of laser parameters on the quality of a laser micromachined feature along with experimental setup and procedure that will reduce their effects.

Fluence

The energy that is delivered to a workpiece is absorbed by free electrons and dissipated by thermal diffusion, and energy transfer by electron-phonon coupling with the workpiece. While femtosecond pulses reduce this phenomenon, the excess energy, or the energy necessary to ionize the material directly illuminated by the beam, is absorbed by the resulting plasma and transferred to the substrate causing temperatures to rise producing a liquid phase which is violently ejected from the machined feature and redeposited on the surface. To reduce this recast layer, the minimum amount of energy should be used during laser micromachining.

Machine Path

Reducing the energy used during laser micromachining will cause the depth of each pass to be reduced, and repeating the machine path will be necessary to produce the desired feature depth. This will also improve the quality of the feature by reducing residual energy in the ion cloud, allowing time for the dissipation of energy transferred to the work surface, and increase the mean free pass of the escaping vapor.

Polarization

We have shown that a linearly polarized beam produces features that are anisotropic when comparing the depths of the produced features. Circularly polarizing the beam causes the center of the beam to produce features with equal depth, but the edges are still slightly skewed when the machining is done by a traversing beam. This effect cannot be avoided but

multi-pass machining will reduce its effects. Many times in thin film micromachining, the films are released from the surface, and the contours of the substrate are irrelevant.

Recommendations for Future Research

Some other influences which are beyond the necessary equipment needed for laser micromachining include magnetic field evacuation of ionized particles to reduce their influence on the workpiece surface. This would include two oppositely charged plates above the machined surface with a strong magnetic field between them. This will draw the ionized material away from the work surface and reduce the interaction time, and thus reduce the residual heat transferred.

Acknowledgements

This author would like to acknowledge the contribution and collaboration of Christian Zorman of Case Western Reserve University for supplying materials used in this research. I would also like to express my appreciation to Iowa State University, Dr. Daniel Bullen, Dr. Gary Tuttle, and especially Pal Molian, whose encouragement and continued support made this research possible.